AGU PUBLICATIONS

JGR

Journal of Geophysical Research: Solid Earth

RESEARCH ARTICLE
10.1002/2016JB013555

Key Points:
- Electrical conductivity of forsterite has large activation energy
- Forsterite conductivity once decreases and then becomes constant with increasing pressure
- Ionic conduction in olivine is dominant conduction mechanism in the upper mantle

Correspondence to:
T. Yoshino,
tyoshino@misasa.okayama-u.ac.jp

Citation:
Yoshino, T., B. Zhang, B. Rhymer, C. Zhao, and H. Fei (2017), Pressure dependence of electrical conductivity in forsterite, *J. Geophys. Res. Solid Earth*, *122*, 158–171, doi:10.1002/2016JB013555.

Received 18 SEP 2016
Accepted 27 DEC 2016
Accepted article online 29 DEC 2016
Published online 14 JAN 2017

Pressure dependence of electrical conductivity in forsterite

Takashi Yoshino[1], Baohua Zhang[2], Brandon Rhymer[3], Chengcheng Zhao[1], and Hongzhan Fei[4]

[1]Institute for Planetary Materials, Okayama University, Misasa, Tottori, Japan, [2]Key Laboratory for High-Temperature and High-Pressure Study of the Earth's Interior, Institute of Geochemistry, Chinese Academy of Sciences, Guiyang, Guizhou, China, [3]Department of Geosciences, State University of New York at Stony Brook, Stony Brook, New York, USA, [4]Bayerisches Geoinstitut, University of Bayreuth, Bayreuth, Germany

Abstract Electrical conductivity of dry forsterite has been measured in muli-anvil apparatus to investigate the pressure dependence of ionic conduction in forsterite. The starting materials for the conductivity experiments were a synthetic forsterite single crystal and a sintered forsterite aggregate synthesized from oxide mixture. Electrical conductivities were measured at 3.5, 6.7, 9.6, 12.1, and 14.9 GPa between 1300 and 2100 K. In the measured temperature range, the conductivity of single crystal forsterite decreases in the order of [001], [010], and [100]. In all cases, the conductivity decreases with increasing pressure and then becomes nearly constant for [100] and [001] and slightly increases above 7 GPa for [010] orientations and a polycrystalline forsterite sample. Pressure dependence of forsterite conductivity was considered as a change of the dominant conduction mechanism composed of migration of both magnesium and oxygen vacancies in forsterite. The activation energy (ΔE) and activation volume (ΔV) for ionic conduction due to migration of Mg vacancy were 1.8–2.7 eV and 5–19 cm^3/mol, respectively, and for that due to O vacancy were 2.2–3.1 eV and −1.1 to 0.3 cm^3/mol, respectively. The olivine conductivity model combined with small polaron conduction suggests that the most part of the upper mantle is controlled by ionic conduction rather than small polaron conduction. The previously observed negative pressure dependence of the conductivity of olivine with low iron content (Fo_{90}) can be explained by ionic conduction due to migration of Mg vacancies, which has a large positive activation volume.

1. Introduction

Electrical conductivity of olivine, which is the most dominant mineral in the upper mantle, has been considered to be controlled by small polaron conduction derived from electron hopping between ferric and ferrous sites [*Schock et al*., 1989; *Hirsch et al*., 1993; *Yoshino*, 2010; *Yoshino et al*., 2012] or proton conduction if olivine contains considerable amounts of hydrogen [*Yoshino et al*., 2006, 2009; *Wang et al*., 2006; *Poe et al*., 2010; *Du Frane and Tyburczy*, 2012; *Yoshino and Katsura*, 2013]. Optical band gaps are of the order of 8 eV for both mantle olivine and forsterite [*Shankland*, 1969; *Nitsan and Shankland*, 1976]. Therefore, intrinsic ionic conduction has been disregarded as the dominant conduction mechanism in olivine under mantle pressure-temperature condition. However, olivine conductivity data show relatively higher activation enthalpies (ΔH^*) above 2 eV in the temperature range above 1600 K at pressures to 13 GPa [*Schock et al*., 1989; *Shankland and Duba*, 1990; *Yoshino et al*., 2006, 2009]. Quantitative defect models have been developed to produce an internally consistent model of defect populations based on the electrical conductivity and thermopower data at room pressure under control of oxygen fugacity [*Hirsch et al*., 1993; *Constable and Roberts*, 1997; *Constable*, 2006]. *Schock et al*. [1989] found that the sign of Seebeck coefficient in olivine changes from negative to positive at 1673 K based on thermopower measurement at 1 atm, suggesting that the dominant electric conduction mechanism switches from small polaron conduction at low temperatures to ionic conduction by formation and migration of magnesium vacancies at high temperatures. Therefore, ionic conduction could be important in the upper mantle with high-mantle potential temperatures (>1700 K). Recent Mg and O self-diffusion data have shown the strong pressure dependence [*Fei et al*., 2016] characterized by positive and negative activation volumes for Mg and O, respectively. Thus, dominant ionic vacancy contributing to the ionic conduction might switch from Mg to O as pressure increases.

Several electrical conductivity measurements on Fe-bearing olivine at high pressures have shown that electrical conductivity decreases with increasing pressure [e.g., *Omura et al*., 1989; *Xu et al*., 2000; *Dai et al*., 2010].

The negative pressure dependence of electrical conductivity requires the positive activation volume for a main conduction mechanism. Although most of the researchers considered small polaron conduction as the dominant conduction mechanism of Fe-bearing olivine in a measurement temperature range, small polaron conduction in main mantle minerals is characterized by a small negative activation volume (olivine and ringwoodite: *Yoshino et al*. [2012]; ferropericlase: *Ohta et al*. [2007] and *Yoshino et al*. [2011]; bridgmanite: *Shankland et al*. [1993], *Goddat et al*. [1999], *Katsura et al*. [2007], *Ohta et al*. [2010], and *Sinmyo et al*. [2014]). The estimated activation volume for small polaron conduction ranges from -0.26 to $-0.55\,cm^3$/mol. The positive activation volume obtained from the conductivity measurement of olivine under high pressure could be influenced by large contribution of ionic conduction to the bulk conductivity in the temperature range for the conductivity measurement. Therefore, knowledge of pressure dependence of the ionic conduction in olivine is needed to understand the electrical structure of the upper mantle.

To elucidate the effect of ionic conduction on the electrical conductivity of olivine, conductivity measurement of forsterite is useful to detect ionic conduction in association with cationic and anionic vacancies by subtraction of the effect of small polaron conduction. Although electrical conductivity measurement of forsterite has been conducted by many researchers [e.g., *Morin et al*., 1977; *Cygan and Lasaga*, 1986; *Schock et al*., 1989], the pressure dependence of forsterite conductivity has not been explored. In the present study, we measured the electrical conductivity of synthetic forsterite single crystal along each principle crystallographic direction and sintered forsterite aggregate at temperatures up to 2100 K and pressures up to 14 GPa. We discuss conduction mechanism in forsterite. Then we will propose a model of the electrical conductivity of iron-bearing olivine as a function of pressure combining with small polaron conduction model of *Constable* [2006]. Finally, we discuss a cause of the negative pressure dependence on electrical conductivity of Fe-bearing olivine and a significance of ionic conduction in olivine under the condition of the Earth's upper mantle.

2. Experimental Methods

Two types of starting material were used for the conductivity measurement. One starting material is a synthetic large forsterite crystal (Oxide Company) grown parallel to *b* axis by the Czochralski technique. The starting samples were cored from the single crystal, with a diameter of 2 mm and a thickness of 0.8 mm, parallel to each principle crystallographic orientation. The other starting material was sintered forsterite aggregates made from stoichiometric oxide mixture (Mg_2SiO_4). The powder was loaded into a Mo capsule and was sintered at 1 GPa and 1273 K for an hour in a piston cylinder apparatus. The sintered material was cored from the center portion with a diameter of 2 mm by an ultrasonic drilling machine. The grain size of the sintered aggregate was around 5 μm. The chemical composition of these starting samples is close to the ideal forsterite stoichiometry, and electron microprobe analysis indicates that concentration of impurities is below the detectable limit. However, chemical analysis of laser ablation inductively coupled plasma–mass spectroscopy showed that the synthetic single crystal contains considerable amount of Ir (~80 wt ppm) and minor amount of Fe (2 wt ppm) [*Fei et al*., 2012]. Fourier transform infrared spectrum shows no presence of O–H bond absorption bands, indicating that the water content is less than 1 wt ppm.

The conductivity measurement was performed in a Kawai-type multi-anvil press. The pressure medium was an octahedral Cr_2O_3-doped MgO pressure medium with a 14 mm edge length. Resistive heating element is a cylindrical $LaCrO_3$ furnace surrounded by ZrO_2 thermal insulator. The cored single crystal was set in a capsule made of sintered MgO aggregates. Two Mo electrodes with a diameter of 2 mm were placed at both sides of the sample. Each Mo electrode connects two independent sets of $W_{97}Re_3$-$W_{75}Re_{25}$ thermocouples, which are electrically insulated from the $LaCrO_3$ furnace by alumina and magnesia insulators. The inner anvils were tungsten carbide cubes with a 6 mm truncation edge length. The detailed cell design for the conductivity measurements is shown elsewhere [*Yoshino et al*., 2008]. The impedance spectroscopic measurements were performed by a pseudo four-wire method using an impedance gain-phase analyzer (Solartron 1260) combined with an interface (Solartron 1296). The amplitude of the applied voltage for alternating current was set to be 1 V. The impedance spectra were obtained in a frequency range of 10^{-1}–10^6 Hz from high to low frequencies.

The samples were compressed in a stepwise fashion with several different press loads (1, 2, 3, 4, and 5.5 MN). Pressures at each load were estimated to be 3.4, 6.7, 9.6, 12.1, and 14.9 GPa, respectively, based on the

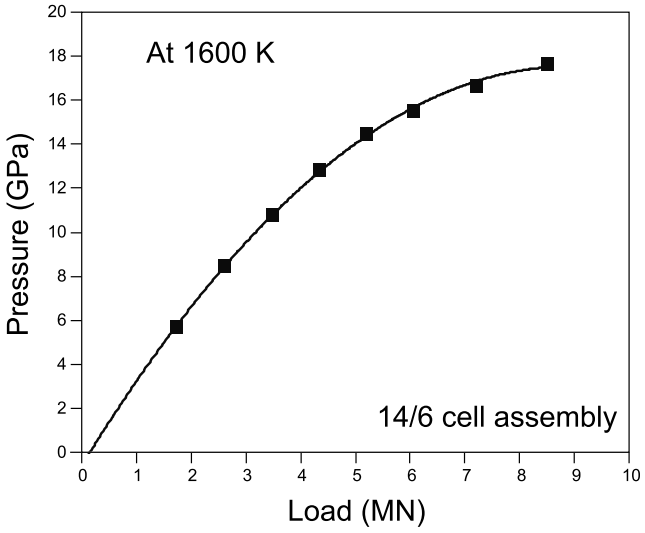

Figure 1. Pressure calibration curve at 1600 K for the 14/6 cell assemblage for electrical conductivity measurement obtained from in situ X-ray diffraction study [*Yoshino et al.*, 2012]. The pressure was determined by MgO pressure scale proposed by *Tange et al.* [2009]. P (GPa) $= -2.2516 \times 10^{-5}$[Load (MN)]$^2 + 0.040293$[Load (MN)] $- 0.43863$. The press load for [111]-type split sphere press installed at Institute for Planetary Materials, Okayama University, is converted from that applied by [100] (DIA)-type press, SPEED MkII installed at BL04B1 at SPring-8.

previous pressure calibration determined by in situ X-ray diffraction study [*Yoshino et al.*, 2012] (Figure 1). Taking into consideration of a slight pressure drop along cooling path [*Yamazaki et al.*, 2012], the error of pressure estimation is around 0.75 GPa. At the desired load, the samples were heated to the maximum temperature (1900–2100 K), and then stepwisely cooled to the temperature as far as we determine the sample resistance for the impedance spectra. The impedance spectra were obtained every 50 K step. After the conductivity measurements at the maximum press load, the samples were quenched and then decompressed at room temperature. The experimental conditions are summarized in Table 1.

Figure 2 shows examples of impedance spectra plotted in a complex impedance plane (a Cole-Cole plot). The impedance spectrum is characterized by a single semicircular arc, suggesting that a simple RC (R-CPE) parallel circuit is considered as equivalent circuit. The sample conductivity (σ (S/m)) was calculated from the dimension of the recovered sample by the equation $\sigma = l/RS$, where l is the sample thickness (m), S is a cross-sectional area of sample (m^2), and R is the measured resistance (Ω). Although the recovered samples have some cracks perpendicular to the cylindrical axis, the sample thickness between two electrodes was kept at the original length within an accuracy of 5 μm. The sample dimension at

Table 1. Summary of Experimental Runs

Run no.	[hkl]	P	T	σ_{0HT}	ΔH_{HT}	σ_{0LT}	ΔH_{LT}
		(GPa)	(K)	(S/m)	(eV)	(S/m)	(eV)
5K2905	[100]	3.4	1300–2000	1.8e8(31)	3.66(30)	21(9)	1.12(5)
		6.7	1200–2050	2.8e8(60)	3.60(38)	3.7(13)	1.01(4)
		9.6	1300–2050	3.4e5(59)	2.84(30)	0.9(7)	0.87(9)
		12.1	1300–2050	1.8e5(30)	2.73(30)	0.5(4)	0.80(11)
		14.9	1300–2050	2.1e5(35)	2.79(29)	0.9(7)	0.89(9)
1K2422	[010]	3.4	1300–2000	4.4e4(38)	2.50(15)	1.9(24)	0.83(14)
		6.7	1500–2100	2.4e6(33)	2.97(24)	0.8(18)	0.77(30)
		9.6	1500–2100	3.0e5(31)	2.69(20)	0.1(2)	0.43(30)
		12.1	1600–2100	1.1e6(9)	2.95(15)	0.2(2)	0.53(13)
		14.9	1600–2100	4.1e4(30)	2.33(13)	n.d.	n.d.
5K2903	[001]	3.4	1300–2050	2.3e5(9)	2.31(6)	0.01(2)	0.14(16)
		6.7	1300–2050	3.1e8(38)	3.70(22)	6.2(13)	0.89(2)
		9.6	1300–2050	7.7e7(94)	3.54(21)	24(6)	1.11(3)
		12.1	1300–2050	2.2e5(23)	3.76(18)	2.07	1.20(2)
		14.9	1300–2050	2.5e9(62)	4.24(43)	118(17)	1.35(2)
A2595[a]	poly	1	1650–1900	5.5e5(57)	2.53(16)		
1K2410		3.4	1450–1900	2.2e5(10)	2.49(6)		
		6.7	1550–2000	3.1e6(6)	2.98(3)		
		9.6	1500–2000	1.7e6(3)	2.88(3)		
		12.1	1500–2000	1.9e4(6)	2.90(3)		

[a]Conductivity measurement was performed in cubic multi-anvil press.

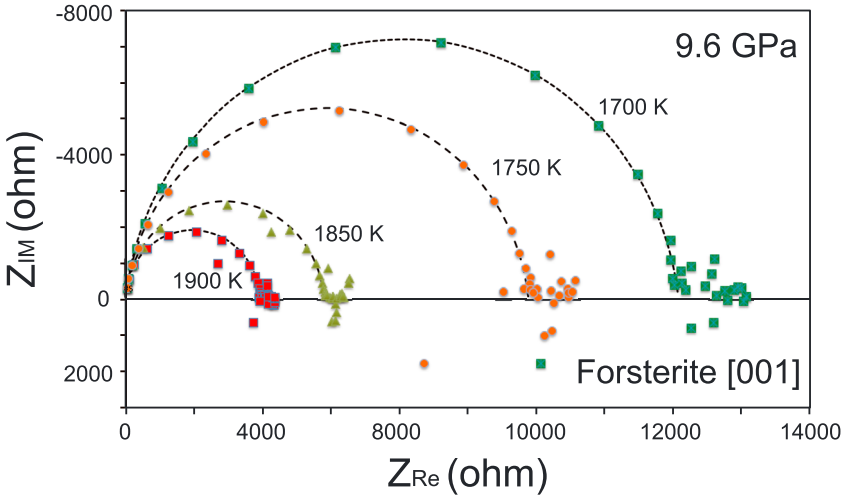

Figure 2. Complex impedance spectra (Cole-Cole plot) at frequencies ranging from 1 MHz to 0.1 Hz at the temperatures indicated. Impedance spectra of forsterite single crystal parallel to [001]. The dotted lines indicate the fittting results of each impedance spectrum by assumption of R-CPE parallel circuit.

high pressure and high temperature was estimated from the change in density of forsterite based on the calculation done by *Xu et al.* [2004]. Both increase and reduction of radial distance and thickness by thermal expansion and pressurization were considered without any thought of the crystal anisotropy. When the conductivity was measured parallel to *b* axis, the error of the estimated conductivity is expected to be the maximum because [010] is not only the most compressible direction by pressurization but also the most expansive direction by heating.

3. Experimental Results

The conductivity (σ)-temperature (T)-pressure (P) relationships can be expressed by the following Arrhenian equation:

$$\sigma = \sigma_0 \exp\left(-\frac{\Delta E + P\Delta V}{kT}\right) \tag{1}$$

where σ_0 is the pre-exponential factor (S/m), ΔE is the activation energy (eV), ΔV is the activation volume (cm^3/mol), k is the Boltzmann constant, and T is the temperature (K). The experimental results are presented in Table 1 and Figures 3 and 4. In all experiments, the electrical conductivity increases with increasing temperature (Figure 3). The electrical conductivity (σ) of the synthetic single crystal is the highest along [001] and decreases in the order $\sigma_{[001]} > \sigma_{[010]} > \sigma_{[100]}$ at any pressures we measured. For the single crystal, the temperature dependence of conductivity is not linear on an Arrhenius plot, with changes in slope at around 1800 K. A change of the activation enthalpy with temperature corresponds to a switch of dominant conduction mechanism. Here two conduction mechanisms are categorized as low- and high-temperature regimes. The conductivities for all samples measured at constant load are best fit by an Arrhenius equation:

$$\sigma = \sigma_{0\mathrm{HT}} \exp\left(-\frac{\Delta H_{\mathrm{HT}}}{kT}\right) + \sigma_{0\mathrm{LT}} \exp\left(-\frac{\Delta H_{\mathrm{LT}}}{kT}\right) \tag{2}$$

where ΔH ($=\Delta E + P\Delta V$) is the activation enthalpy (eV) and subscripts HT and LT denote high- and low-temperature regimes. ΔH_{HT} determined from experimental data obtained during cooling ranges from 2.3 to 3.7 eV, whereas ΔH_{LT} are relatively low and around 1 eV (Table 1). Figure 5 shows pressure variations of ΔH_{HT} and ΔH_{LT}. On the other hand, the electrical conductivity of the sintered aggregate shows no kink in Arrhenius plot and is plotted in a range of conductivity anisotropic variation in a high-temperature regime defined from single crystal measurement. The activation enthalpy is quite consistent with ΔH_{HT} along [010].

Figure 4 shows the electrical conductivity obtained for forsterite samples at various temperatures as a function of pressure. The electrical conductivity of all samples largely decreases with increasing pressure at

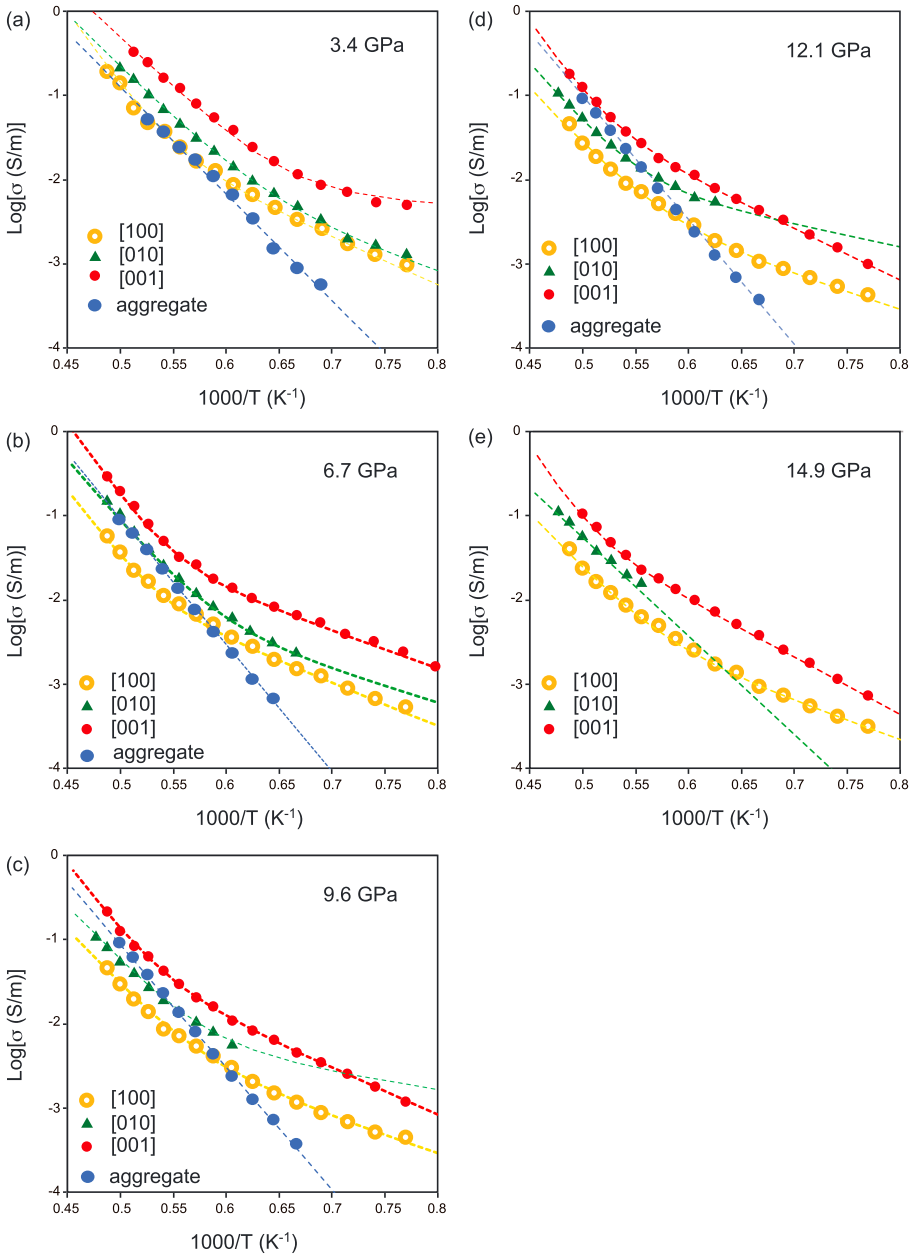

Figure 3. Electrical conductivities (log σ) of Mg_2SiO_4 samples plotted as a function of reciprocal temperature (K^{-1}) at (a) 3.4 GPa, (b) 6.7 GPa, (c) 9.6 GPa, (d) 12.1 GPa, and (e) 14.9 GPa. The dashed lines denote the electrical conductivity calculated by data fitting based on equation (2). Note that the electrical conductivity of single crystal forsterite increases in an order of [100], [010], and [001] and that of the sintered forsterite aggregate shows absence of the low-temperature regime.

constant temperatures up to 7 GPa. Above 7 GPa, the conductivity becomes almost constant with pressure, and the conductivity of [010] direction and a sintered aggregate slightly increases with pressure above 10 GPa. A large decrease of conductivity below 7 GPa at constant temperature indicates that the activation volume (ΔV) is large and positive.

A comparison of the Arrhenius relations reported in the previous studies on electrical conductivity data of forsterite is shown in Figure 5. The conductivity data in this study for synthetic forsterite were relatively obtained at higher temperatures than those of previous studies [*Pluschkell and Engell*, 1968; *Shankland*, 1969; *Duba*, 1972; *Morin et al.*, 1977; *Schock et al.*, 1989]. ΔH_{HT} calculated from this study at various pressures agree with those obtained above 1500 K by *Pluschkell and Engell* [1968], *Shankland* [1969], and *Schock et al.*

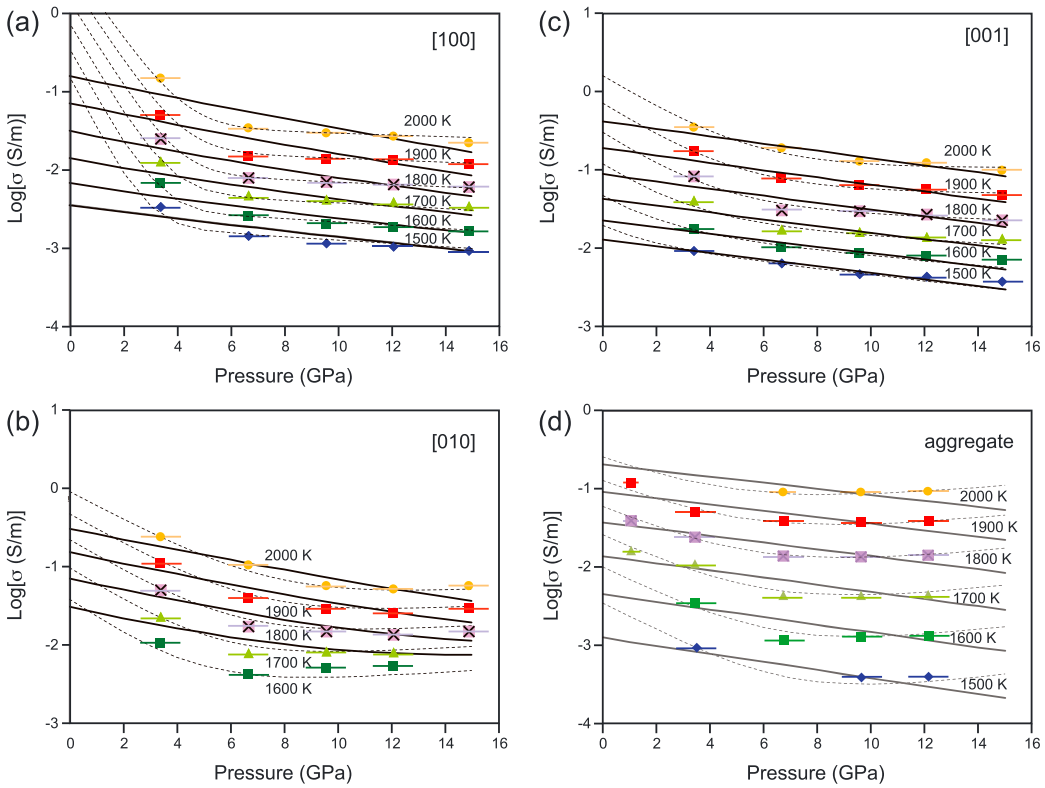

Figure 4. Electrical conductivities of forsterite (Mg_2SiO_4) as a function of pressure at variable temperatures. (a) Single crystal forsterite parallel to [100]. (b) Single crystal forsterite parallel to [010]. (c) Single crystal forsterite parallel to [001]. In general, the conductivity of forsterite constantly decreases with increasing pressure at constant temperature up to 7 GPa. The dashed lines indicate the electrical conductivity calculated by data fitting based on equation (4) as a function of temperature and pressure. The solid lines represent the fitting results without consideration of oxygen vacancy. The fitted parameters in Table 2 were used for this calculation.

[1989]. However, the extrapolation of the literature data sets to higher temperatures shows that our data are higher than theirs. Some studies found a change in activation energy of the electrical conductivity in olivine and forsterite at around 1500 K. At higher temperatures above 1500 K, the activation enthalpy becomes higher than 2 eV. ΔH_{HT} (2.3–3.7 eV) determined at constant load for the conductivity of the synthetic forsterite single crystal along any direction are consistent with those (2–3.25 eV) reported by *Morin et al.* [1977]. The measured temperature range for the previous conductivity measurements is too low to allow precise determination of the activation enthalpy for the dominant conduction mechanism at high temperatures accurately. In the overlapped temperature range, the conductivity values of synthetic single crystal for each principle crystallographic direction are fairly higher than those obtained by *Schock et al.* [1989]. Most of the previous studies at room pressure used either DC or multifrequency electric bridge limiting methods, leading to considerable electrode polarization. Thus, the measured resistance might be significantly lower than that determined from the impedance spectroscopy.

4. Discussion

4.1. Conduction Mechanism

Intrinsic ionic conduction for cation and anion vacancies is difficult to constrain from only the electrical conductivity data because the conductivity of the synthetic forsterite is strongly controlled by small amounts of impurities. Here intrinsic conduction means a pure semiconductor without any significant impurity or dopant species present. A change of activation enthalpy was observed within the temperature range in this study, implying that all measurements on the conductivity of single crystal were in at least two different regimes. At higher temperatures, the ΔH_{HT} exceeds 2 eV at any pressure, whereas the ΔH_{LT} (~1 eV) observed only in the single crystal for each crystallographic direction is comparable to that (1.13 eV) determined from the

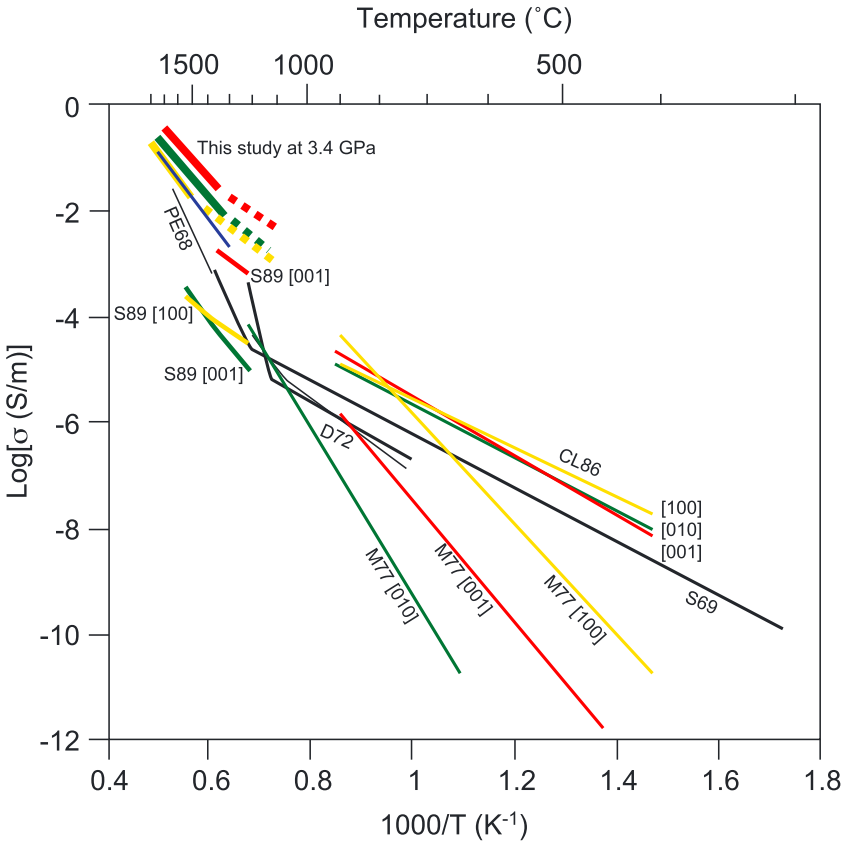

Figure 5. Comparison of the electrical conductivity of forsterite with prrevious studies in Arrhenius plot. Abbreviations: PE68, *Pluschkell and Engell* [1968]; S69, *Shankland* [1969]; D72, *Duba* [1972]; M77, *Morin et al.* [1977]; CL86, *Cygan and Lasaga* [1986]; S89, *Schock et al.* [1989].

low-temperature part of *Shankland* [1969], which was interpreted as extrinsic. The activation enthalpy (ΔH) is composed of an enthalpy of formation of the thermally activated defect (ΔH_f) and an enthalpy of migration of defects to neighboring sites (ΔH_m). At high temperatures, ΔH_f becomes a dominant factor controlling the activation enthalpy.

Various studies on various types of diffusion for Mg, O, and Si in forsterite or olivine at 1 bar have shown that Mg self-diffusion is the fastest among the other elements (Si and O). Mg vacancy can be the most probable charge carrier governing the electrical conductivity of forsterite. Substantial experimental and theoretical works have reported Mg diffusivities in forsterite and olivine. For example, the activation energy for migration of Mg vacancies was determined to be 1.52 eV based on Fe-Mg interdiffusion along [010] measured in the temperature range of 873–1173 K [*Jaoul et al.*, 1995]. At relatively higher temperatures (1273–1573 K), the activation energy for Mg tracer diffusion was determined to be 4.15 ± 0.62 eV [*Chakraborty et al.*, 1994]. The activation energy for Fe-Mg interdiffusion determined at 12 GPa and in higher temperature range (1623–1823 K) was 3.59 ± 0.61 eV [*Holzapfel et al.*, 2007]. Computational studies suggested that activation energies for intrinsic Mg diffusion controlled mostly by formation of defect or interstitial in forsterite are significantly high (3.9 eV, *Jaoul et al.* [1995]; 5.35 eV along [001] and [010] and 4.01 eV along [100], *Walker et al.* [2009]). For formation of Mg vacancy in forsterite, a Frenkel defect composed of a pair of an interstitial site $Mg_i^{\bullet\bullet}$ and V''_{Mg} is considered to be an energetically favorable defect rather than a Schottky defect composed of a pair of V''_{Mg} and $V_O^{\bullet\bullet}$ [*Jaoul et al.*, 1995; *Walker et al.*, 2009]. The present conductivity measurement demonstrates that the activation enthalpies (ΔH_{HT}) are slightly smaller but consistent with those obtained from the Mg self-diffusion within an error range.

The present results demonstrate that electrical conductivity is anisotropic in the synthetic forsterite single crystal. The highest conductivity along [001] is consistent with the conductivity measurement results of

olivine and forsterite at atmospheric pressure by *Schock et al*. [1989]. The fastest crystallographic direction of Fe-Mg interdiffusion and Mg tracer diffusion is also along [001], which is a factor of 4–8 times faster than along [100] and [010] [*Chakraborty et al*., 1994; *Chakraborty*, 1997; *Dohmen et al*., 2007]. Considering the energy of vacancy formation in forsterite, the M1 site for Mg vacancies is more favorable than the M2 site [*Béjina et al*., 2009]. The diffusion path between two adjacent M1 vacant sites along [001] is predicted to have lower activation energy compared to [100] and [010] [*Walker et al*., 2009]. Thus, the anisotropic feature showing the highest conductivity along [001] also supports a presence of ionic conduction mechanism involving V''_{Mg} as a dominant charge carrier.

Previous experimental and computational studies have shown strong negative pressure dependence on Mg diffusion in olivine. The activation volume for Fe-Mg interdiffusion is determined to be 4–7 cm^3/mol in olivine and forsterite diffusion couple [*Misener*, 1974; *Holzapfel et al*., 2007]. Pressure dependence of Mg tracer diffusivity in forsterite measured to 10 GPa yields a relatively smaller activation volume of approximately 1–3.5 cm^3/mol [*Chakraborty et al*., 1994]. Computer simulation results yielded the large activation volume (ΔV) for Frenkel defect formation enthalpy of forsterite to be around 5 cm^3/mol and the small activation volume less than 1 cm^3/mol for migration [*Jaoul et al*., 1995; *Béjina et al*., 2009]. Up to 7 GPa, large reduction of the conductivity is in good agreement with strong pressure dependence determined from Mg diffusion studies and indicates that only the migration energy of Mg vacancy, which has almost zero activation volume, cannot account for the large pressure dependence observed in lower pressure range. Thus, defect formation energy should contribute to high positive activation volume for electrical conduction in synthetic forsterite at high temperatures.

The present results demonstrate that pressure dependence on electrical conductivity becomes smaller at higher pressures and the conductivity parallel to [010] occasionally increases at more than 10 GPa. Thus, small effect of pressure on electrical conductivity at above 7 GPa cannot attribute to only the charge carrier of Mg vacancy. Another possible candidate of charge carrier contributing to the electrical conductivity of synthetic forsterite at high pressures could be oxygen vacancies. Although diffusion coefficients of oxygen (D_O) are distinctly lower than that of Mg (D_{Mg}) at 1 bar, *Fei et al*. [2014] predicted a tiny difference between them based on measurement of D_O at 8 GPa. The activation volume for D_O under dry conditions has not been reported and assumed from 0 to 7 cm^3/mol, which is comparable to the activation volume of D_{Mg} [*Costa and Chakraborty*, 2008]. However, a recent experimental study on pressure dependence on D_O in dry forsterite yields a negative activation volume [*Fei et al*., 2016]. Unlike Mg diffusion, there is compelling experimental evidence that both the self-diffusion coefficients and the activation energy for oxygen diffusion between forsterite and natural olivine are isotropic [*Costa and Chakraborty*, 2008; *Dohmen et al*., 2007; *Jaoul et al*., 1980]. As shown in Figure 2, a conductivity difference between [001] and the other directions tends to decrease with increasing pressure. This series of evidence implies that dominant charge carrier in the synthetic forsterite changes from Mg vacancies to oxygen vacancies at pressures higher than 7 GPa.

The experimentally determined activation energies for D_O of dry forsterite ranging from 2.8 to 3.5 eV [*Andersson et al*., 1989; *Dohmen et al*., 2002; *Gérard and Jaoul*, 1989; *Jaoul et al*., 1980; *Ryerson et al*., 1989] agree with those of electrical conductivity determined above 7 GPa (2.3–4.2 eV). Computational simulation suggested that the intrinsic activation energies for D_O considering summation of the fraction of the defect formation (e.g., Schottky or Frenkel) energy required to form the diffusing species and the extrinsic activation energy are much larger (5.09 eV) than the activation energies determined by all conductivity and diffusion experiments [*Walker et al*., 2003]. To interpret the discrepancy, *Walker et al*. [2003] also predicted that the activation energies for the oxygen interstitial formed by a presence of impurities are 3.21, 3.89, and 3.02 eV along [100], [010], and [001], respectively. These values are somewhat higher than those calculated from the conductivity data obtained at higher pressures, while the anisotropy in activation energy also disagrees with the present results. Therefore, the constant conductivity at high pressures attributes to the ionic conduction controlled by the mixed state of diffusion of magnesium and oxygen vacancies.

The electrical conductivity of a mineral is a summation of the various conduction mechanisms, i.e.,

$$\sigma = \sum_j N_j q_j \mu_j \tag{3}$$

where N_j is the density of the jth type of charge carrier, q_j is the effective charge ($q = ze$), and μ_j is its mobility. Each conduction mechanism has the characteristic activation energies required for the charge

Table 2. Fitting Parameters

Run no.	Sample	σ_{0Mg} (S/m)	ΔE_{Mg} (eV)	ΔV_{Mg} (cm^3/mol)	σ_{0O} (S/m)	ΔE_O (eV)	ΔV_O (cm^3/mol)	σ_{0m} (S/m)	ΔE_m (eV)	ΔV_m (cm^3/mol)
5K2905	[100]	1.1e5(6)	1.75(23)	18.6(56)	1.3e6(52)	3.05(21)	0.3(3)	1.6 (6)	0.87(4)	0.6(1)
		7.5e5(131)	2.63(28)	3.4(5)				3.4(25)	0.98(8)	0.4(2)
1K2422	[010]	3.4e5(35)	2.38(11)	6.9(5)	1.1e4 (4)	2.23(6)	−0.8(3)	7.0 (70)	0.88(10)	−0.6(4)
		2.0e5(35)	2.31827)	2.684)				0.05(22)	0.46(44)	−0.8(11)
5K2903	[001]	1.0e7(14)	2.71(22)	8.3(17)	1.7e6(19)	2.93(21)	−0.3(4)	7.2(25)	0.83(4)	1.2(0)
		1.4e7(25)	3.01(30)	2.0(2)				14(7)	0.91(6)	1.2(1)
1K2410	Poly	6.2e4(4)	2.16(11)	5.3(7)	2.2e6(5)	3.07(8)	−1.1(5)			
		1.0e6(4)	2.66(6)	1.5(1)						

concentration and mobility. In addition, there are also temperature and pressure dependences of a defect concentration for various types of charge carrier [*Poirier*, 1999]. Here we model the pressure dependence of electrical conductivity of forsterite (σ_{Fo}) in terms of two ionic conduction mechanisms derived from Mg and O self-diffusion as follows:

$$\begin{aligned}\sigma_{Fo} &= \sigma_{Mg} + \sigma_{Ox} + \sigma_{LT} \\ &= \sigma_{0Mg}\exp\left(-\frac{\Delta E_{Mg} + P\Delta V_{Mg}}{kT}\right) + \sigma_{0Ox}\exp\left(-\frac{\Delta E_{Ox} + P\Delta V_{Ox}}{kT}\right) + \sigma_{0LT}\exp\left(-\frac{\Delta E_{LT} + P\Delta V_{LT}}{kT}\right),\end{aligned} \quad (4)$$

where σ_{Mg} and σ_{Ox} are electrical conductivity derived from Mg and O vacancies, respectively, and σ_{0Mg} and σ_{0Ox}, ΔE_{Mg} and ΔE_{Ox}, and ΔV_{Mg} and ΔV_{Ox} are pre-exponential factor, activation energy, and activation volume for electrical conductivity derived from Mg and O vacancies, respectively. All the conductivity data were fitted by equation (4). For comparison, the data fitting was also performed for the case that oxygen vacancy has no contribution to the bulk ionic conductivity of forsterite. The fitting parameters are summarized in Table 2.

For each run, variations of conductivity values as a function of temperature and pressure can explain the present data well (Figure 4) when we consider contribution of the oxygen vacancy, whereas when we consider only the Mg vacancy, the fitting curves cannot reproduce the measurement data, and the fitting parameters yield large error. For the high-temperature regime, the ΔE_{Mg} of the single crystal forsterite is comparable to the ΔE_{Ox}, whereas the ΔV_{Mg} is much higher than the ΔV_{Ox}. The activation volumes for the electrical conduction in association with Mg vacancies (ΔV_{Mg}) are large and positive (6–18 cm^3/mol) and are slightly higher or comparable to those of the Mg diffusion experiments [*Béjina et al*., 2009]. Relatively higher ΔV_{Mg} would be caused by absence of lower pressure data in this study (<3.5 GPa). The ΔV_{Ox} are relatively small and negative except for along [100], which is consistent with a result of the latest study on oxygen self-diffusion [*Fei et al*., 2016]. On the other hand, the fitting parameters for the low-temperature regime determined from the synthetic single crystal show no significant variation for each crystallographic direction. ΔE_{LT} are 0.8–0.9 eV. The small ΔV_{LT} are consistent with that (<1 cm^3/mol) for migration of Mg self-diffusion [*Jaoul et al*., 1995; *Béjina et al*., 2009].

The synthetic forsterite single crystal used by this study is not truly pure and contains considerable amount of Fe and Ir. *Chakraborty et al.* [1994] noted the fO_2 dependence of Mg tracer diffusion in nominally pure (very low Fe content: 120–180 ppm) forsterite, suggesting that the absolute values of diffusivities depend on concentrations of impurities, that is, ferrous or ferric iron. Small polaron conduction characterized by electron hole hopping between ferrous and ferric iron is unlikely to be dominant charge carrier at such low iron concentration [*Yoshino et al*., 2012]. Indeed the maximum concentration of iron for this composition cannot produce number of the charge carrier enough to satisfy the measured conductivity values even if $Fe^{3+}/\Sigma Fe$ is 0.5.

For iron-bearing olivine, Mg diffusion has significantly lower activation energies (~2 eV) [*Chakraborty et al*., 1994; *Chakraborty*, 1997; *Dohmen et al*., 2007] because the Mg vacancies can be formed under lower energetic cost. In the presence of iron, a number of possible reactions can create defects at magnesium sites. Mg vacancies are formed by maintenance of charge neutrality in association with the oxidation of iron or by the incorporation of ferric iron. This process can be represented by the reaction [*Walker et al*., 2009]:

$$Fe_2O_3 + 3Mg_{Mg}{}^{x} \rightarrow 2Fe_{Mg}{}^{\bullet} + V_{Mg}{}'' + 3MgO \quad (5)$$

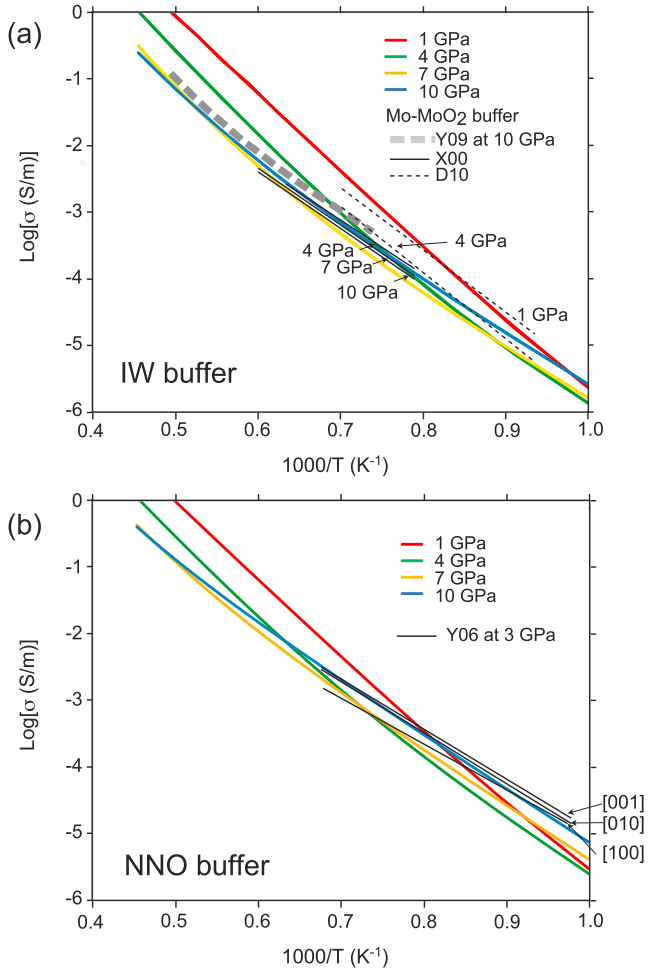

Figure 6. Electrical conductivity of olivine Fo_{90} in Arrhenius plot as a function of pressure as a summation of ionic conduction calculated from equation (8) and small polaron conduction calculated from the model of *Constable* [2006] under different oxygen buffer conditions. (a) Fe-FeO (IW) buffer. The dashed thick line shows the electrical conductivity of olivine aggregates (Fo_{91}) determined at 10 GPa [*Yoshino et al.*, 2009]. The thin and dashed solid lines denote the electrical conductivity of olivine aggregates (Fo_{90}) and olivine compact (Fo_{88}) measured at different pressure conditions [*Xu et al.*, 2000; *Dai et al.*, 2010]. (b) Ni-NiO (NNO) buffer. The calculated electrical conductivity under IW buffer compares with those of single crystal olivine (Fo_{92}) determined at 3 GPa [*Yoshino et al.*, 2006].

For pyroxene buffered sample, more realistic reaction process in the upper mantle is as follows:

$$Fe_2O_3 + MgSiO_3 + 3Mg_{Mg}^{x} \rightarrow 2Fe_{Mg}^{\bullet} + V_{Mg}'' + 3Mg_2SiO_4 \quad (6)$$

The [001] migration energy yields an activation energy of 2.21 or 1.99 eV for reactions (5) and (6), respectively [*Walker et al.*, 2009]. These activation enthalpy values are slightly lower than the activation enthalpy determined from the high-temperature regime. One possibility to account for intermediate activation enthalpy (2–3 eV) would be the mixed state of formation energy and migration energy in the measurement temperature range.

Another potential charge carrier in the synthetic forsterite could be produced during crystal growth process. If all iron in the synthetic forsterite is oxidized to the trivalent state, loss of magnesium and creation of a V''_{Mg} defect would occur simultaneously to maintain charge neutrality through the irreversible reaction [*Schock et al.*, 1989]:

$$Mg_{Mg}^{\times} + 2Fe_{Mg}^{\times} \rightarrow 2Fe_{Mg}^{\bullet} + V''_{Mg} + Mg\downarrow \quad (7)$$

The synthetic crystal also contains considerable amount of Ir (~80 wt ppm). The presence of Ir also can create a V''_{Mg} defect through the following reaction [*Schock et al.*, 1989]:

$$Mg_{Mg}^{\times} + Ir_{Mg}^{\times} \rightarrow Ir_{Mg}^{\cdot\cdot\cdot} + V''_{Mg} + Mg\downarrow \quad (8)$$

This type of pre-existing defect is a permanent deficiency independently of oxygen fugacity. The present results showing higher conductivity values especially for the low-temperature regime observed in the synthetic single crystal than the previous studies (Figure 4) might represent high concentration of V''_{Mg} created during synthesis of the single crystal. Since the conductivity measurement of the forsterite aggregates synthesized from oxide mixture shows no sign of the low-temperature regime, the low-temperature regime appeared in the single crystal could be caused by high defect density due to the Ir contamination in the single crystal synthesized by using Ir crucible. Therefore, the low-temperature regime is not considered in the following discussion to construct the mantle olivine conductivity model.

4.2. Cause of Negative Pressure Dependence of Iron-Bearing Olivine

Several works have investigated the effect of pressure on electrical conductivity of dry olivine. Based on the conductivity measurement for olivine along forsterite-fayalite join, *Yoshino et al.* [2012] demonstrated that

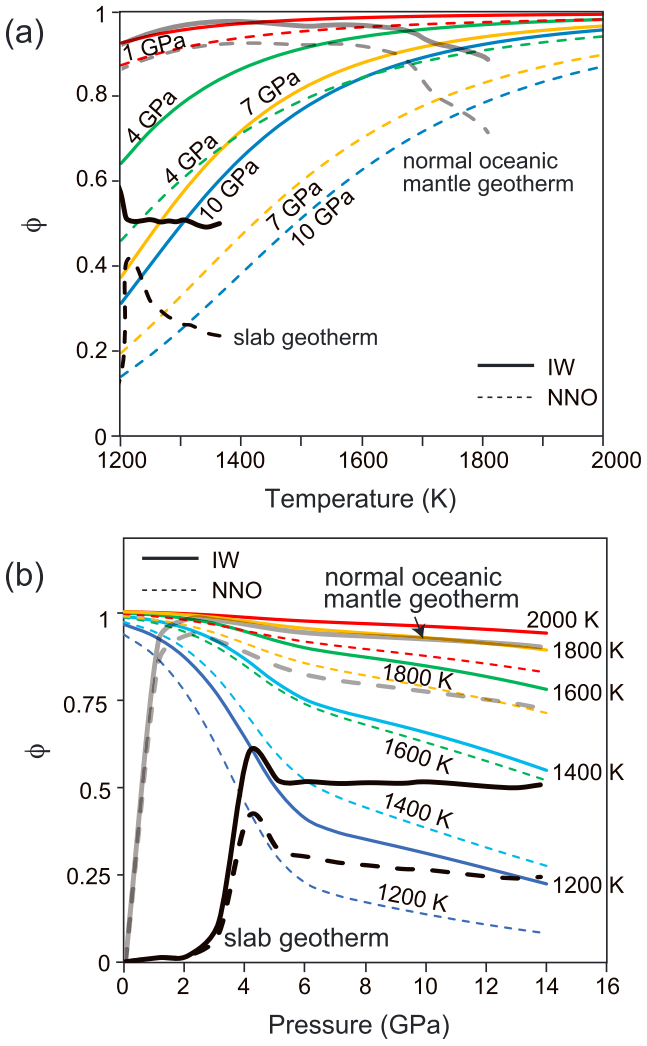

Figure 7. Proportion of ionic conduction contributing to the bulk electrical conductivity for $(Mg_{0.90},Fe_{0.10})_2SiO_4$ olivine (φ) as a function of (a) temperature and (b) pressure under the upper mantle condition. The thin solid and dashed curves indicate the calculated values under Fe-FeO and Ni-NiO buffers, respectively. The thick curves labeled "oceanic normal geotherm" denote variation of φ along geotherms of 30 Ma oceanic mantle based on a recent model [*Katsura et al.*, 2010]. The gray thick curves labeled "slab geotherm" indicate variation of φ along geotherm from the Cascadia subduction zone based on the model by [*Wada and Wang*, 2009].

the activation volume for the conductivity of dry olivine has a small negative value and increases to $-0.67\,cm^3$/mol with increasing X_{Fe}. However, for olivine with low X_{Fe} (~0.1), several workers have reported a positive activation volume based on conductivity measurements over a relatively wide pressure range ($12.72\,cm^3$/mol, *Omura et al.* [1989]; $0.68\,cm^3$/mol, *Xu et al.* [2000]) and in a restricted pressure range (1–4 GPa, $25\,cm^3$/mol) [*Dai et al.*, 2010]. The electrical conductivity for small polaron conduction is defined by

$$\sigma_h = \frac{gN_{Fe}c(1-c)q^2a^2v}{kT}\exp\left(-\frac{\Delta E_h}{kT}\right), \tag{9}$$

where g is a geometric factor close to unity, N_{Fe} is the number density of iron, c is the fraction of ferric iron over total iron content, q is an elementary charge, a is the jump distance, v is the lattice vibrational frequency responsible for hopping, and ΔE_h is the hopping energy [*Poirier*, 1999]. Since pressurization leads to decrease of the lattice parameter, the jump distance for electron hole hopping becomes shorter as pressure increases. Indeed, most of the previous conductivity measurements of major ferromagnesian mantle minerals have reported a negative activation volume for small polaron conduction as described before. *Yoshino et al.* [2009] noted that the conductivity values of the dry olivine aggregates (Fo_{90}) measured at 10 GPa were nearly the same as those calculated from the SEO3 model of *Constable* [2006] without consideration of pressure effect. Thus, the activation volume seems to be negligibly small when the X_{Fe} in olivine is low. In conclusion, the negative pressure dependence of low X_{Fe} olivine would be affected by ionic conduction of Mg vacancies characterized by a large positive activation volume. Otherwise the positive activation volumes reported by previous studies might be an experimental artifact by the sample dehydration during repeated heating.

Next we quantitatively consider the effect of ionic conduction on conductivity of the mantle olivine (Fo_{90}). The electrical conductivity of dry Fe-bearing olivine can be approximated as a summation of ionic and small polaron conductions. Models of dry olivine electrical conductivity as a function of temperature and oxygen fugacity have been established as a standard model of dry San Carlos olivine (Fo_{90}) based on the conductivity measurement at room pressure [*Constable et al.*, 1992]. *Constable* [2006] proposed a new model "Standard Electrical Olivine 3 (SEO3)" by taking quantitative estimates of mobility and concentration for magnesium vacancies and small polarons at high temperatures into account. The SEO3

model yields conductivity values similar to many laboratory data measured at high pressures. However, the effect of pressure on concentration and mobility of Mg and O vacancies was not considered in this model. To calculate the conductivity of olivine with composition relevant to the normal upper mantle (Fo_{90}), we used the present results (equation (8)) for ionic conduction of the high-temperature regime and the SEO3 model for small polaron conduction. For small polaron conduction, the activation volume is assumed to be 0 cm^3/mol. The bulk conductivity was calculated from the geometric mean of the conductivity in the three crystallographic directions ($\sigma_{bulk} = (\sigma_{[100]}\sigma_{[010]}\sigma_{[001]})^{1/3}$).

Figure 6 shows variations of electrical conductivity in Arrhenius plot as a function of pressure at different oxygen buffer conditions (Fe-FeO (IW) and Ni-NiO). The conductivity values under IW buffer are lower than those under relatively higher oxygen fugacity condition. Ionic conduction largely decreases with increasing pressure up to 7 GPa, whereas small polaron conduction slightly increases with increasing pressure because oxygen fugacity increases with increasing pressure at the same oxygen buffer. The calculated conductivity values are in agreement with the experimental data. In the temperature and pressure range measured by *Xu et al*. [2000] and *Dai et al*. [2010], a tendency that the conductivity slightly decreases with increasing pressure is quite consistent with their results showing a small positive activation volume. Thus, the negative pressure dependence of the olivine conductivity reported by previous works attributes to the large contribution of ionic conduction to the Fe-bearing olivine conductivity. On the other hand, the conductivity under Ni-NiO buffer increases with increasing pressure below 1600 K.

Figure 7 shows the proportion of ionic conduction (σ_{ion}) to the bulk conductivity ($/\sigma_{bulk}$) ($\varphi = \sigma_{ion} / \sigma_{bulk}$) as a function of temperature and pressure for each oxygen buffer. For each buffer, the φ increases with increasing temperature because of a large activation enthalpy for ionic conduction (Figure 7a), whereas the φ decreases with increasing pressure because of a large positive activation volume for ionic conduction at pressures lower than 5 GPa (Figure 7b). Ionic conduction is dominant along the normal mantle geotherm because of small contribution of small polaron conduction due to the small amount of ferric iron content, whereas small polaron conduction is dominant along the slab geotherm [*Wada and Wang*, 2009]. Recent high-pressure petrological studies have shown that the oxygen fugacity decreases with increasing pressure in association with accommodation of ferric iron in garnet and reaches iron saturation condition above 7 GPa [e.g., *Rohlbach et al*., 2007; *Stagno et al*., 2013]. Thus, ionic conduction could be the most dominant conduction mechanism in olivine throughout the upper mantle rather than small polaron conduction except for the subduction zone. However, we did not consider the effect of oxygen fugacity on ionic conduction. More investigation is necessary to clarify this effect.

Acknowledgments
Constructive comments by W. Du Frane and an anonymous reviewer were useful to improve this manuscript. We are grateful to D. Yamazaki for discussions of this research and L. Chao and C. Oka for experimental assistant. This work was supported by a Grant-in-Aid for Scientific Research (24244087) and JSPS MEXT/KAKENHI grant JP15H05827 to T.Y. from the Japan Society for the Promotion of Science. It was also supported by the internship program (MISIP15) of the Institute for Study of the Earth's Interior, Okayama University. The data for this paper are available by contacting the corresponding author (T.Y.: tyoshino@misasa.okayama-u.ac.jp) upon request.

References

Andersson, K., G. Borchardt, S. Scherrer, and S. Weber (1989), Self-diffusion in Mg_2SiO_4 (forsterite) at high temperature, *Fresenius' Z. Anal. Chem.*, *333*, 383–385.
Béjina, F., M. Blanchard, K. Wright, and G. D. Price (2009), A computer simulation study of the effect of pressure on Mg diffusion in forsterite, *Phys. Earth Planet. Inter.*, *172*, 13–19.
Chakraborty, S. (1997), Rates and mechanisms of Fe–Mg interdiffusion in olivine at 980–1300°C, *J. Geophys. Res.*, *102*, 12,317–12,331, doi:10.1029/97JB00208.
Chakraborty, S., J. R. Farver, R. A. Yund, and D. C. Rubie (1994), Mg tracer diffusion in synthetic forsterite and San Carlos olivine as a function of *P*, *T* and fO_2, *Phys. Chem. Miner.*, *21*, 489–500.
Constable, S. (2006), SEO3: A new model of olivine electrical conductivity, *Geophys. J. Int.*, *166*, 435–437.
Constable, S., and J. J. Roberts (1997), Simultaneous modeling of thermopower and electrical conduction in olivine, *Phys. Chem. Miner.*, *24*, 319–325.
Constable, S. C., T. J. Shankland, and A. Duba (1992), The electrical conductivity of an isotropic olivine mantle, *J. Geophys. Res.*, *97*, 3397–3404, doi:10.1029/91JB02453.
Costa, F., and S. Chakraborty (2008), The effect of water on Si and O diffusion rates in olivine and implications for transport properties and processes in the upper mantle, *Phys. Earth Planet. Inter.*, *166*, 11–29.
Cygan, R. T., and A. C. Lasaga (1986), Dielectric and polarization behavior of forsterite at elevated temperatures, *Am. Mineral.*, *71*, 758–766.
Dai, L., H. Li, C. Li, H. Hu, and S. Shan (2010), The electrical conductivity of dry polycrystalline olivine compacts at high temperatures and pressures, *Mineral. Mag.*, *5*, 849–857.
Dohmen, R., S. Chakraborty, and H. W. Becker (2002), Si and O diffusion in olivine and implications for characterizing plastic flow in the mantle, *Geophys. Res. Lett.*, *29*(21), 2030 doi:10.1029/2002GL015480.
Dohmen, R., H.-W. Becker, and S. Chakraborty (2007), Fe–Mg diffusion in olivine I: Experimental determination between 700 and 1,200°C as a function of composition, crystal orientation and oxygen fugacity, *Phys. Chem. Miner.*, *34*, 389–407.
Du Frane, W. L., and J. A. Tyburczy (2012), Deuterium-hydrogen exchange in olivine: Implications for point defects and electrical conductivity, *Geochem. Geophys. Geosyst.*, *13*, Q03004, doi:10.1029/2011GC003895.
Duba, A. (1972), Electrical conductivity of olivine, *J. Geophys. Res.*, *77*, 2483–2495, doi:10.1029/JB077i014p02483.

Fei, H., C. Hegoda, D. Yamazaki, M. Wiedenbeck, H. Yurimoto, S. Shcheka, and T. Katsura (2012), High silicon self-diffusion coefficient in dry forsterite, Earth Planet. *Sci. Lett.*, *345*, 95–103.
Fei, H., M. Wiedenbeck, D. Yamazaki, and T. Katsura (2014), No effect of water on oxygen self-diffusion rate in forsterite, *J. Geophys. Res. Solid Earth*, *119*, 7598–7606, doi:10.1002/2014JB011141.
Fei, H., M. Wiedenbeck, N. Sakamoto, H. Yurimoto, T. Yoshino, D. Yamazaki, and T. Katsura (2016), Negative activation volume of oxygen self-diffusion in forsterite paper presented at 2016 Fall Meeting, AGU, San Francisco, Calif., 12–16 Dec.
Gérard, O., and O. Jaoul (1989), Oxygen diffusion in San Carlos olivine, *J. Geophys. Res.*, *94*, 4119–4128, doi:10.1029/JB094iB04p04119.
Goddat, A., A. Peyronneau, and J. P. Poirier (1999), Dependence on pressure of conduction by hopping of small polarons in minerals of the Earth's lower mantle, *Phys. Chem. Miner.*, *27*, 81–87.
Hirsch, L. M., T. J. Shankland, and A. G. Duba (1993), Electrical conductivity and polaron mobility in Fe-bearing olivine, *Geophys. J. Int.*, *114*, 36–44, doi:10.1111/j.1365-246X.1993.tb01464.x.
Holzapfel, C., S. Chakraborty, D. C. Rubie, and D. J. Frost (2007), Effect of pressure on e-Mg, Ni and Mn diffusion in $(Fe_xMg_{1-x})SiO_4$ olivine, *Phys. Earth Planet. Inter.*, *162*, 186–198.
Jaoul, O., C. Froidevaux, W. B. Durham, and M. Michaut (1980), Oxygen self-diffusion in forsterite: Implications for the high-temperature creep mechanism, *Earth Planet. Sci. Lett.*, *47*, 391–397.
Jaoul, O., Y. Bertran-Alvalez, R. C. Liebermann, and G. D. Price (1995), Fe–Mg interdiffusion in olivine up to 9 GPa at T = 600–900°C; experimental data and comparison with defect calculations, *Phys. Earth Planet. Inter.*, *89*, 199–218.
Katsura, T., A. Yoneda, D. Yamazaki, T. Yoshino, and E. Ito (2010), Adiabatic temperature profile in the mantle, *Phys. Earth Planet. Inter.*, *183*, 212–218.
Katsura, T., S. Yokoshi, K. Kawabe, A. Shatskiy, M. Okube, H. Fukui, E. Ito, A. Nozawa, and K. Funakoshi (2007), Pressure dependence of electrical conductivity of $(Mg,Fe)SiO_3$ ilmenite, *Phys. Chem. Miner.*, *34*, 249–255.
Misener, D. J. (1974), Cationic diffusion in olivine to 1400°C and 35 kbar, in *Geochemical Transport and Kinetics*, edited by A. W. Hofmann et al., pp. 117–129, Carnegie Institution of Washington, Washington, D. C.
Morin, F. J., J. R. Oliver, and R. M. Housley (1977), Electrical properties of forsterite, Mg_2SiO_4, *Phys. Rev. B*, *6*, 4434–4445.
Nitsan, U., and T. J. Shankland (1976), Optical properties and electronic structure of mantle silicates, *Geophys. J. R. Astron. Soc.*, *45*, 59–87.
Ohta, K., K. Hirose, S. Onoda, and K. Shimizu (2007), The effect of iron spin transition on electrical conductivity of magnesiowüstite, *Proc. Jpn. Acad., Ser. B*, *83*, 97–100.
Ohta, K., K. Hirose, S. Onoda, and K. Shimizu (2010), The electrical resistance measurements of $(Mg,Fe)SiO_3$ perovskite at high pressures and implications for electronic spin transition of iron, *Phys. Earth Planet. Inter.*, *180*, 154–158.
Omura, K., K. Kurita, and M. Kumazawa (1989), Experimental study of pressure dependence of electrical conductivity of olivine at high temperatures, *Phys. Earth Planet. Inter.*, *57*, 291–303.
Pluschkell, V. W., and H. J. Engell (1968), Ionen und Elektronenleitung im Magnesium Orthosilikat, *Ber. Dtsch. Keram. Ges.*, *45*, 388–394.
Poe, B. T., C. Romano, F. Nestola, and J. R. Smyth (2010), Electrical conductivity anisotropy of dry and hydrous olivine at 8 GPa, *Phys. Earth Planet. Inter.*, *181*, 103–111.
Poirier, J. P. (1999), *Introduction to the Physics of the Earth's Interior*, 2nd ed., p. 312, Cambridge Univ. Press, Cambridge, U. K.
Rohlbach, A., C. Ballhaus, U. Golla-Schindler, P. Ulmer, V. S. Kamenetsky, and D. V. Kuzmin (2007), Metal saturation in the upper mantle, *Nature*, *449*, 456–458.
Ryerson, F. J., W. B. Durham, D. J. Cherniak, and W. A. Lanford (1989), Oxygen diffusion in olivine: Effect of oxygen fugacity and implications for creep, *J. Geophys. Res.*, *94*, 4105–4118, doi:10.1029/JB094iB04p04105.
Schock, R. N., A. G. Duba, and T. J. Shankland (1989), Electrical conduction in olivine, *J. Geophys. Res.*, *94*, 5829–5839, doi:10.1029/JB094iB05p05829.
Shankland, T. J. (1969), Transport properties of olivines, in *The Application of Modern Physics to the Earth and Planerary Interiors*, *NATO Adv. Study Inst.*, edited by S. K. Runcorn, pp. 175–190 , Wiley-Interscience, New York.
Shankland, T. J., and A. Duba (1990), Standard electrical conductivity of isotropic, homogeneous olivine in the temperature range 1200°–1500°C, *Geophys. J. Int.*, *103*, 25–31.
Shankland, T. J., J. Peyronneau, and J. P. Poirier (1993), Electrical conductivity of the Earth's lower mantle, *Nature*, *366*, 453–455.
Sinmyo, R., G. Pesce, E. Greenberg, C. McCammon, and L. Dubrovinsky (2014), Lower mantle electrical conductivity based on measurements of Al, Fe-bearing perovskite under lower mantle conditions, *Earth Planet. Sci. Lett.*, *393*, 165–172.
Stagno, V., D. O. Ojwang, C. A. McCammon, and D. J. Frost (2013), The oxidation state of the mantle and the extraction of carbon from Earth's interior, *Nature*, *493*, 84–88.
Tange, Y., Y. Nishihara, and T. Tsuchiya (2009), Unified analyses for P-V-T equation of state of MgO: A solution for pressure-scale problems in high P-T experiments, *J. Geophys. Res.*, *114*, B03208, doi:10.1029/2008JB005813.
Wada, I., and K. Wang (2009), Common depth of slab-mantle decoupling: Reconciling diversity and uniformity of subduction zones, *Geochem. Geophys. Geosyst.*, *10*, Q10009, doi:10.1029/2009GC002570.
Walker, A. M., K. Wright, and B. Slater (2003), A computational study of oxygen diffusion in olivine, *Phys. Chem. Miner.*, *30*, 536–545.
Walker, A. M., S. M. Woodley, B. Slater, and K. Wright (2009), A computational study of magnesium point defects and diffusion in forsterite, *Phys. Earth Planet. Inter.*, *172*, 20–27.
Wang, D., M. Mookherjee, Y. Xu, and S. Karato (2006), The effect of water on the electrical conductivity of olivine, *Nature*, *443*, 977–980.
Xu, Y., T. J. Shankland, and A. G. Duba (2000), Pressure effect on electrical conductivity of mantle olivine, *Phys. Earth Planet. Inter.*, *118*, 149–161.
Xu, Y., T. J. Shankland, S. Linhardt, D. C. Rubie, F. Langenhorst, and K. Klansinski (2004), Thermal diffusivity and conductivity of olivine, wadsleyite and ringwoodite up to 20 GPa and 1373 K, *Phys. Earth Planet. Inter.*, *143–144*, 321–226.
Yamazaki, D., et al. (2012), P-V-T equation of state for ε-iron up to 80 GPa and 1900 K using the Kawai-type high pressure apparatus equipped with sintered diamond anvils, *Geophys. Res. Lett.*, *39*, L20308, doi:10.1029/2012GL053540.
Yoshino, T. (2010), Laboratory electrical conductivity measurements of mantle minerals, *Surv. Geophys.*, *31*, 163–206.
Yoshino, T., and T. Katsura (2013), Electrical conductivity of mantle minerals: Role of water in conductivity anomalies, *Annu. Rev. Earth Planet. Sci.*, *41*, 605–628.
Yoshino, T., T. Matsuzaki, S. Yamashita, and T. Katsura (2006), Hydrous olivine unable to account for conductivity anomaly at the top of the asthenosphere, *Nature*, *443*, 973–976.
Yoshino, T., T. Matsuzaki, A. Shatzkiy, and T. Katsura (2009), The effct of water on the elctrical conductivity of olivine aggregates and its implications for the electrical structure of the upper mantle, *Earth Planet. Sci. Lett.*, *288*, 291–300.

Yoshino, T., M. Nishi, M. Matsuzaki, D. Yamazaki, and T. Katsura (2008), Electrical conductivity of majorite garnet and its implications for electrical structure of the mantle transition zone, *Phys. Earth Planet. Inter.*, *170*, 193–200.

Yoshino, T., E. Ito, T. Katsura, D. Yamazaki, S. Shan, X. Guo, M. Nishi, Y. Higo, and K. Funakoshi (2011), Effect of iron content on electrical conductivity of ferro-periclase with implications for the spin transition pressure, *J. Geophys. Res.*, *116*, B04202, doi:10.1029/2010JB007801.

Yoshino, T., A. Shimojuku, S. Shan, X. Guo, D. Yamazaki, E. Ito, Y. Higo, and K. Funakoshi (2012), Effect of temperature, pressure and iron content on the electrical conductivity of olivine and its high-pressure polymorphs, *J. Geophys. Res.*, *117*, B08205, doi:10.1029/2011JB008774.